Original Research Article

International journal of spray and combustion dynamics

International Journal of Spray and Combustion Dynamics
2023, Vol. 15(1) 51–69

DOI: 10.1177/17568277221151141
journals.sagepub.com/home/scd
SAGE

E-POD investigations of turbulent premixed flame dynamics approaching lean blow-out conditions

Roberto Meloni[1], Nicola Chiarizia[2], Pier Carlo Nassini[2] and Antonio Andreini[2]

Abstract

Thanks to the continuous computational power increase, the use of high-fidelity computational fluid dynamics (CFD) simulations is nowadays customary, especially in the gas turbines design process. The extraordinary temporal and spatial detail of such analyses generate large datasets, which must be carefully studied to correlate different quantities and gain information to characterize the behavior of combustor designs. Several advanced post-processing tools have been proposed; however, the Extended-POD (E-POD) holds the greatest potential for turbulent combustion applications when the mutual influence of different quantities is the main goal of the investigation. The present work investigates the application of the E-POD to an LES model of a perfectly-premixed, swirl-stabilized, methane-air flame approaching Lean-Blow-Out. Leveraging the validation against the experimental data at two different operating conditions on a laboratory test case, the numerical model has been used to collect several quantities of interest for shedding light on the flow-flame interaction near the blow-out. The post-processing algorithm has been used to highlight the differences between two conditions approaching the extinction at distinct air-flow velocities. It has been found that, when the burner is operated with a higher velocity, the flame is subjected to a cyclic low-frequency breakdown around the internal recirculation zone, leading to an ingestion of cold products from the external parts of the combustor toward the center. Although other local effects acting on the flame brush have been found in both conditions, they are related mainly to higher order coherent structures with a lower energy content. As a result, their impact onto flame stability is found to be of secondary importance since their limited interaction with flame stabilization. The work shows that E-POD represents a powerful tool for investigating the key features of flame dynamics even at near-blow-out conditions, constituting a valid algorithm for interpreting the results of CFD analyses on gas turbines combustors.

Keywords

E-POD, turbulent premixed flame, LBO, LES, flame dynamics

Date received: 1 September 2022; accepted: 28 December 2022

Introduction

The modern optical measurement techniques as well as the more and more accurate Computational Fluid Dynamics codes are nowadays able to generate very complex sets of data requiring advanced analysis tools to be only partially post processed.[1–3] Especially in combustion, the most recent optical diagnostics can be employed to provide not only information about the flow field through multi-dimensional particle image velocimetry measurements but also high frequency acquisitions of the reactant species distribution via natural chemiluminescence or induced fluorescence.[4,5] From the numerical standpoint, the adoption of high-fidelity multi-physics approaches is paving the way to the so-called "virtual testing" that provides the possibility to extract the same kind of information in any desired location of the three-dimensional domain: in this case the

[1]Baker Hughes, Gas Turbine Technology, Florence, Italy
[2]Department of Industrial Engineering, DIEF, University of Florence, Florence, Italy

Corresponding author:
Antonio Andreini, Department of Industrial Engineering, DIEF, University of Florence, Florence, 50139, Italy.
Email: antonio.andreini@unifi.it

management of the fluxes of data can become even more challenging.[6,7] The availability of all these data can be leveraged trying to correlate different quantities and gain information aiming to characterize the behavior of a given combustor design in a wide range of operating conditions. Eventually, specific hardware modifications and improvements could be conceived once the correlation between different phenomena is found.

Depending on the physics to be studied, different advanced post-processing techniques (or their combinations) can be applied with the goal to extract as many information as possible. When dealing with the dynamics of the flame-flowfield interaction, traditionally a fraction of the frequency content is retained and investigated. The simplest technique of this kind is represented by the phase-locked average having the acquisitions sampled at a fixed frequency.[8] Such post-processing can shed some light on the physical correlation of different quantities characterized by the same periodicity. The main drawback of this approach is that the dominant frequency must be periodic and, more importantly, known a-priori.

The most powerful post-processing tool for characterizing a data set from the dynamic point of view is the Dynamic Mode Decomposition (DMD).[1,9] Here, a discrete set of frequencies is used to decompose the acquired data base; the advantage of such approach is that each decomposing mode is associated to one single frequency able to identify a coherent structure, although not providing any information about its energy content.[6,10,11] Several works in literature have demonstrated the ability of such approach in identifying the correlation between the flowfield structures and the flame front. Most of them are related to the investigation of the thermo-acoustic instabilities where usually a limited number of frequencies are excited by the coupling of the heat release rate and acoustic pressure at the natural frequencies of the combustion system.

Huang et al.[7,12] tested different numerical techniques for the study of the self-excited instabilities in a hybrid RANS/LES model of a longitudinal laboratory-scaled lean combustor, trying to identify the physical mechanisms behind the interaction between the acoustic waves and the unsteady heat release. It is demonstrated that the DMD is the only algorithm able to directly correlate any unstable frequency to the fluid-dynamic behavior of the system. The application of the DMD to the numerical data set of the heat release, axial velocity and fuel mass fraction revealed how the sixth longitudinal mode was triggered by the Processing Vortex Core (PVC) hydrodynamic instability, while the coupling of the Vortex Breakdown Bubble (VBB) with the acoustics of the system was responsible for the excitation at higher frequency. An even more innovative approach is proposed by Carlsson et al.[6] with the application of an extended DMD formulation to the study of the flowfield-flame interaction of a lean premixed low-swirl stabilized flame. The novelty of the proposed approach consists in the projection of the G-equation used for the flame front identification in a LES context onto the DMD based built through the velocity field. In such way, the coherent structures of the flow at specific frequencies are extracted along with the associated flame structures: this allowed to prove how the flame stabilization is enhanced by vortices at the inner shear layer recurring at frequencies characterizing both the flowfield and the flame.

An alternative approach for the investigation of the flowfield-flame interaction is represented by the Proper Orthogonal Decomposition.[13,14] The POD is a powerful tool to detect and isolate the most energetic coherent structures in a given data set even if it is only qualitatively able to provide information about the relationship among quantities of different nature. In literature, several research papers applied both numerically and experimentally such technique. Petersson et al.[15] leverage simultaneous PIV and OH-PLIF measurements in a low swirl injector trying to recognize common patterns between the flow filed and the flame location.

Gadiraju et al.[16] used the POD for the post-processing of flame images of an industrial gas turbine nozzle. The detection of the main features characterizing the combustion fluctuations represented the main goal of this work: it is demonstrated how the large-scale coherent flow structures (i.e., the PVC) are crucial for the self-sustained combustion instabilities even close to the lean blow-out of the flame. A similar investigation was carried out by Boxx et al.[17] in a dual-swirl combustor. Stereo-PIV and OH-PLIF measurements are used to identify the behavior of the turbulence-chemistry interaction in the inner recirculation zone and in the inner shear layer of the flame. The FFT of the experimental signals are exploited to find an analogy with the frequency content of the time coefficients from the POD when the system is subjected to a low-frequency instability: it is found that the first three modes are affected by both the frequency associated to the hydrodynamic instability and the acoustically triggered frequency.

An innovative variation of the POD is presented by Iudiciani et al.[18] In presence of a periodic instability like in the case of self-excited dynamics, the authors proposed a Phase-Averaged POD to be applied to the time coefficients of each mode. Once applied to the experimental images of OH-chemiluminescence, this approach allows a better understanding of the impact of each mode onto the physics of the combustion instability. Furthermore, the procedure doesn't need to know a-priori the dominant frequency of the phenomenon since this is an outcome of the time-coefficient post-processing.

An even more valid option compared to the POD is represented by the Extended-POD.[19,20] Such post-processing can be performed through the projection of a second quantity onto the POD base of the primary and it is particularly useful to reveal their intimate interconnection in a quantitative and more analytically formal way,

especially when there is no predominant set of frequencies in the system.

The present research paper investigates about the application of the latter post-processing tool to an LES model of a perfectly premixed highly swirled flame approaching the lean extinction limits.[21] Indeed, the lean blow-out of a flame is a major concern with lean-premixed combustion systems, as it limits the operating range of the machine. Although the driving mechanisms which initiate the blow-out are still not completely explained,[22] some key fluid mechanical and kinetic processes associated to the LBO have been identified in the literature. Specifically, the swirl-stabilized flames exhibit consistent local extinctions and modifications of the central recirculation zone, similarly to what observed for bluff-body stabilized flames.[23] More recent studies observed that the local flame extinctions allow the fresh mixture to enter the inner recirculation zone, promoting the progressive fragmentation of the flame sheet and finally leading to the flame root detachment and blow-out.[24] Thus, the LBO is inherently associated to large-scale fluctuations of the flame, making the analysis of the results complex without the appropriate post-processing tools.

Among the different techniques, the E-POD is selected for different reasons. First of all, despite the presence of a low-frequency instability typical of the lean blow out, this does not represent the main mechanism to be investigated and therefore different approaches (like the DMD) do not represent the best way to fully understand the complex phenomenon leading to the flame extinction, characterized by an intimate correlation between flame stretch, flow stabilization and heat release. Analogously, being the extinction affected by such many quantities, the POD stand alone is not able to provide reliable insights about their mutual influence.

The content of the paper is structured as follows. Paragraph 2 will be dedicated to the mathematical formulation of the EPOD and how it has been used to investigate the behavior of the flame approaching the LBO in the present paper. The experimental set up and the operating conditions selected for the LES analysis will be introduced in the Paragraph 3. A brief summary about the combustion model and the numerical set up will be reported in Paragraph 4. The last section will discuss the numerical findings and the corresponding physical insights.

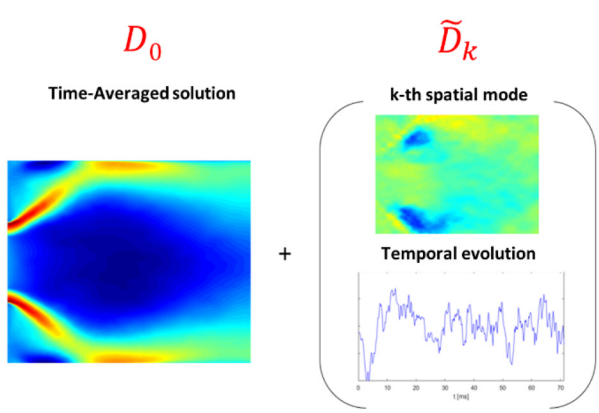

Figure 1. Schematic process to quantify the effect of a POD/E-POD mode onto the time-average solution of a quantity.

POD and extended-POD fundamentals

The Proper Orthogonal Decomposition represents one of the most used algorithm for the detection of coherent structures in turbulent flows,[3,13,25] allowing a given data set of acquisitions $D(x, t)$, describing only the fluctuating part of a phenomenon, to be decomposed into a combination of orthogonal basis, or modes, function exclusively of space $\phi_k(x)$ and time $\psi^T(t)$, each one with a different energy content σ_k:

$$D(x, t) = \sum_k \phi_k(x) a_k(t) = \sum_k \phi_k(x) \sigma_k \psi_k^T(t) \tag{1}$$

These quantities are here calculated according to the so-called snapshot-method introduced by Sirovich et al.[26] In this approach, once N different numerical or experimental samplings have been collected, the problem is reduced to find the eigenvalues σ_k and the eigenvectors $\psi^T(t)$ of the cross-correlation matrix K, built according to Eq. 2.

$$K = D^T D \tag{2}$$

Especially when the dimension of the data base is extremely large, it can be decided to compute only the first $\breve{N}$ eigenvalues of the cross-correlation matrix: this truncation leads to a percentage error in the reconstruction of the fluctuating part of the solution that can be limited when $\breve{N} \to N$.

Independently from the number of eigenvalues, the corresponding POD spatial modes can be finally computed as follows (Eq. 3):

$$\Phi = D \Psi_D \Sigma_\sigma^{-1} \tag{3}$$

where Σ_σ^{-1} is a diagonal matrix containing the square of the energy coefficients σ_k and Ψ_D is the matrix of the temporal modes. With the goal to exploit the POD for the detection of the turbulent structures having an impact onto the flame extinction, the contribution of the $k-th$ mode $\tilde{D}_k = \phi_k(x)\sigma_k\psi_k^T(t)$ can be isolated from Eq. 1. One powerful way to quantify the effect of the generic mode $\tilde{D}_k$ is to algebraically sum it to the time-average field of the quantify under investigation (Figure 1).

It this way, it is possible to verify if that mode can significantly alter the mean field and, in case, in which way. In fact, when the flame is close to the lean blow-out, the time average stand-alone solution doesn't represent an effective and exhaustive information to discriminate which transient effect can eventually lead to the loss of flame. At the same time, if each coherent structure is analyzed stand-alone, it

is not possible to quantify how much impact it has onto the global behavior of the flame.

Additionally, exactly the same procedure can be replicated considering not the generic $k-th$ POD mode but the $k-th$ Extended-POD mode.[19] When different quantities are intimately correlated each other, like in the complex dynamic leading to the flame extinction, the E-POD is an even more powerful algorithm to highlight the mutual influence of different parameters. Mathematically, the E-POD consists in projecting a second set of data $\alpha(x, t)$ onto the eigenvectors of the primary quantity $D(x, t)$. So, the first step of the procedure consists in the calculation of the POD of the primary quantity in order to retrieve the matrix Ψ_D and Σ_σ^{-1}. The second step is the projection of the second quantity onto the first set that can be performed by simply substituting the time acquisition matrix $\alpha(x, t)$ to $D(x, t)$in $Eq.$ (3) such that the corresponding modes are calculated as follows:

$$\phi^\alpha(x) = \alpha\Psi_D\Sigma_\sigma^{-1} \tag{4}$$

Acting in this way, it is possible to isolate the coherent structures, i.e., the Extended POD modes, of the second quantity that are exclusively synchronized with the primary as demonstrated.[20]

As third and final step, the classic POD of the second quantity has to be calculated as well in order to retrieve the corresponding time coefficients that are necessary to calculate the temporal evolution of the generic mode according to the following equation:

$$\tilde{D}_{E-k} = \phi^\alpha(x)\sigma_\alpha\psi_k^T(t) \tag{5}$$

The scheme presented in Figure 1 can be so replicated taking into account the time-averaged field of the secondary quantity and the single E-POD mode calculated according to Eq.4. From a computational perspective, there is practically no difference between the standard POD and the E-POD: the latter approach simply requires more time for the calculation of two PODs and the corresponding cross-correlation summarized by Eq. 4.

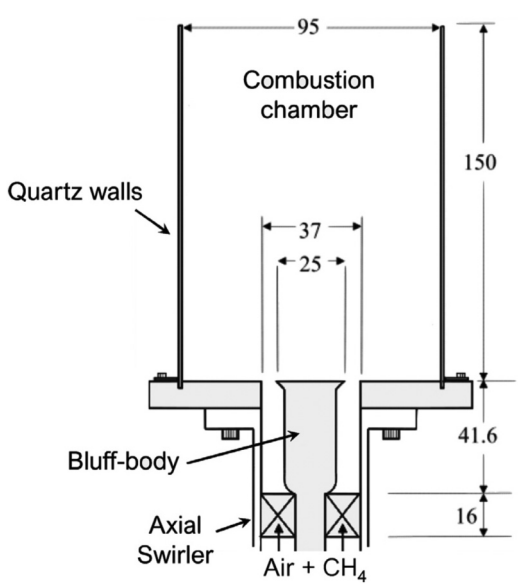

Figure 2. Sketch of the Cambridge atmospheric rig for perfectly premixed gaseous fuels. The dimensions reported in the figure are in mm.

Despite the simplicity of such approach, there are few studies using this methodology, mainly applied to experimental data like in the case of Duwig et al.[27] or mixed numerical-experimental data.[28] As per the authors' knowledge, such approach has never been proposed to deeply analyze the data coming from numerical simulations of turbulent flames close to the lean blow out limit. Moreover, such methodology can be particularly useful from design standpoint: supposing that a specific behavior of the system is mainly correlated to the evolution of a coherent structure (i.e., of a POD mode), the introduction of a design modification conceived to suppress it can be verified through this kind of analysis.

Experimental test rig

The Cambridge flame is here investigated at two different operating conditions just prior the lean extinction to retrieve physical insights on the flow-flame interaction leading to the loss of flame event. This test rig has been extensively used in the past for this kind of characterization with both liquid fuel and natural gas[24,29]: the findings presented in this work are related to the numerical model derived for perfectly mixed reactants and pure methane as fuel gas.[21] Figure 2 shows a longitudinal section of the atmospheric rig consisting of a high swirl-number burner ($S_N = 1.23$) having an external diameter of $D_e = 37\,mm$ and a central bluff body with an internal diameter of $D_b = 25\,mm$. The squared section flame tube is made of quartz allowing detailed optical measurements of both the flame and the flow. The reacting mixture can be studied through both OH-PLIF (at 5 kHz of acquisition frequency) and OH chemiluminescence while LDA technique is used to characterize the flow field.

Experimentally, the LBO is reached through a constant reduction of the fuel gas flow rate starting from a stable operating condition. During this ramp (ϕ depletion equal to -2% every 10 s), several test conditions are acquired and fully characterized through the measurements. Two main bulk velocity levels have been investigated during the tests, as reported in Figure 3: the conditions H1 and P3 represent the LBO limits meaning that in these conditions a stable combustion is detectable, but a further reduction of the equivalence ratio leads to the loss of flame. The impact of the bulk velocity on the ϕ_{LBO} value is clearly identifiable: higher velocities of the flow are responsible for higher local strain of the mixture that reaches the extinction in richer conditions. From the numerical point of view, the LES simulations are able to capture this trend.[21]

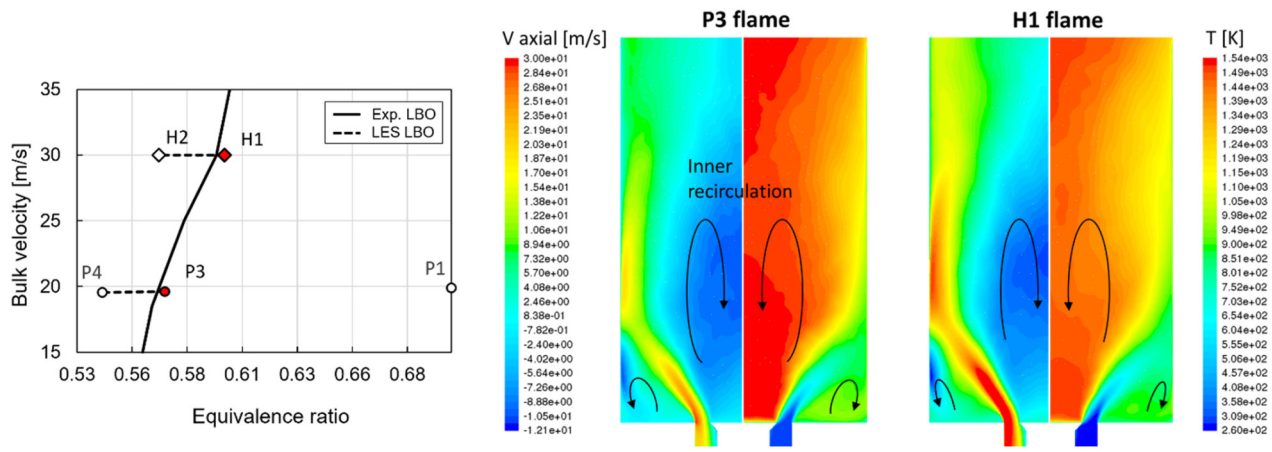

Name	Case	U_b [m/s]	ϕ	ϕ/ϕ_{LBO}	$\dot{m}$ [g/s]
P3	Just Prior LBO	19.6	0.57	100.6%	13.3
H1	Just Prior LBO	30.0	0.6	100.6%	20.4

Figure 3. Experimental LBO curve and the results of the numerical model presented in[21,30] (Top). Main test conditions characterizing the H1 and P3 test points used for the numerical investigation (Bottom).

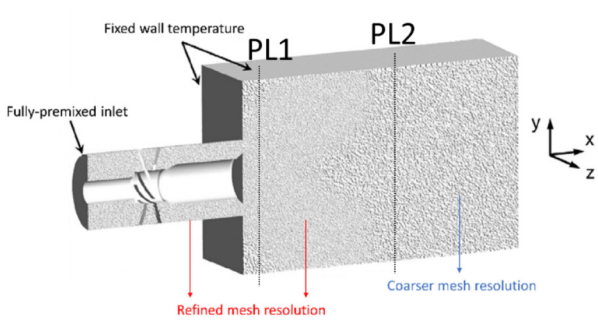

Figure 4. Computational domain related to the premixing duct with the swirler and the combustion chamber. The finer mesh resolution is applied to the premixing duct and the primary zone of the flame tube. The section shows the longitudinal and the two cross planes (PL1, PL2) where the snapshots have been collected: PL1 is located 2 mm downstream burner exit section while PL2 is one chamber diameter downstream the same section.

Additionally, the LBO is reached reducing the equivalence ratio of approximately the same amount in both cases (H2 and P4 conditions in Figure 3).

Numerical model

Computational domain and boundary conditions

The computational domain includes a portion of the mixing duct upstream the swirler, the swirler and the entire flame tube. Additionally, a hemispherical far field is placed downstream in order to simulate the atmospheric discharge allowing to minimize both the reflection of acoustic waves toward the flame and the interaction between the inner recirculation zone (IRZ) and the outlet, being the height of the quartz quite short.

Figure 4 reports the main features of the computational domain that consists of about 7 million polyhedral elements. The picture highlights also the details of the different mesh resolutions applied along the model. The size of 0.5 mm is associated to the swirler and the primary zone, 1 mm for the rest of the combustor while an even more coarse mesh is generated in the far field to increase also the acoustic damping at the outlet section (not reported in Figure 4). Such mesh resolution allows to resolve at least the 80% of the turbulent kinetic energy in the regions of interest, allowing to reproduce the flowfield correctly.[21]

A mass flow inlet type having the mixture fraction value in agreement with the experimental conditions of the test point H1 and P3 and at ambient temperature is adopted. A priori assessment of the wall temperatures is performed for the dome and the quart to take the heat loss into account in the primary zone: the adopted values are $T_{W,Dome} = 773\,K$ and $T_{W,Chamer} = 953\,K$, respectively. The other walls are kept adiabatic. Regarding the far field, a pressure inlet at 1 bar is used for the co-flow surrounding the quartz walls and a standard pressure outlet for the hemisphere.

Combustion model

Although LES resolves most of the turbulent eddies, the characteristic scale of the flame front is still of the same order of magnitude of the mesh size, so an appropriate

model for describing the sub-grid turbulence-chemistry interaction is needed. With this aim, here the Flamelet Generated Manifold (FGM) model is adopted for modeling the turbulent flame using as control variables the reaction progress c based on CO and CO_2 and the mixture fraction Z. A table of the thermo-chemical quantities is generated in Ansys Fluent by solving 1D laminar flamelets with the detailed reaction mechanism GRImech 3.0,[30] and stored as a function of the reaction progress c and the mixture fraction Z. To account the turbulence-chemistry interaction, the table is then integrated by prescribing β-shaped probability density functions, providing a multi-dimensional manifold of the temperature, density and species mass fractions depending on the resolved and sub-grid variances of the two control variables.

Since the flame is near the lean blow-out conditions, a key element of the combustion model is the ability to capture local extinction phenomena, which progressively induce the blow-out. The main effects responsible for the local quenching of the flame, i.e., stretch and heat loss, are mostly lost with the chemistry tabulation, so a dedicated closure is required for reintroducing the dependence of the overall reaction rate on those phenomena. Therefore, in this work the progress variable source term is modeled through the Extended Turbulent Flame Closure (ETFC), following.[21] The ETFC describes the reaction progress source term $\bar{\omega}_c$ by assuming a thin flame front according to turbulent flame closure concept:

$$\bar{\omega}_c = \rho_u S_t |\nabla \tilde{c}| \tag{6}$$

with ρ_u the density of unburned gas and S_t the turbulent flame speed. The latter can be expressed as:

$$S_t = A\, u'^{3/4}_{\Delta} S_c^{1/2} \alpha^{-1/4} (C_s \Delta)^{1/4} \tag{7}$$

where u'_{Δ} is the sub-grid scale velocity fluctuation, C_s the Smagorinsky constant, $\Delta = \sqrt[3]{V_{cell}}$ the mesh cell size, α the thermal diffusivity, S_c the laminar stretched flame consumption speed and $A = 1$ a model constant.

The model prescribes the laminar consumption speed S_c of the flame as a 3d look-up table to embed the stretch κ and heat losses effects on the reaction rate:

$$S_c = S_c(z, \kappa, T_b) \;\; with \;\; pressure, \;\; T_{unburnt} fixed \tag{8}$$

The values of S_c are calculated by solving 1D premixed counterflow flamelets with GRImech 3.0 and multicomponent diffusion, simulating the effects of strain and heat losses by varying independently the jets velocity and the burnt gas temperature. The table is then stored in RAM memory at the beginning of the simulation and accessed by the computational fluid dynamics (CFD) solver for calculating the progress variable source term, according to the local values of stretch and heat losses. Those values require specific algebraic relations depending on the velocity gradients and enthalpy defect on the flame front, not reported here for sake of conciseness. More details about the model the reader are provided,[21] as they applied here without modifications.

The FGM-ETFC model represents a cost-efficient solution to describe localized quenching effects on the flame and demonstrated a good accuracy when applied to extremely lean flames, capturing the blow-out limits within few percentage points of equivalence ratio.

According to the author's experience and to the technical literature on LBO events in typical gas turbine lean premixed combustion regimes, it can be pointed out that LES can be considered an adequate approach for this type of analysis. During the transient process bringing flame to blow-out, it can be observed the onset of low frequency flame fluctuations linked to large scale flow structures which are properly handled by LES. Regarding the turbulent flowfield, the LBO event it's not expected to induce smaller scales and the reduction of overall reaction rate is associated to a thickening of the flame front permitting an even more accurate turbulent flame resolution by LES.

Data acquisition for POD

A time step size equal to $\Delta t = 7.5e-06\ s$ is used during the LES simulation. This value ensures a high stability to the run being the corresponding CFL number below the unity in the entire domain. The sampling rate for the acquisition of the POD snapshots is set to 25 time steps, equal to a frequency of 5.3 kHz. The snapshots used for the post processing have been acquired over a range of 170 ms: assuming a potential low frequency phenomenon related to the loss of flame of 100 Hz as order of magnitude, the simulation length is 17 times this oscillation period.

Three locations are used to collect the data: the mid longitudinal plane and two cross sections at 10 mm and 55 mm from the premixer head, respectively. The first cross section aims to investigate in detail what happens at the flame root while the second is useful to better characterize, together with the longitudinal plane, how the inner-recirculation zone (IRZ) behaves. In fact, close the LBO limit the flame morphology is characterized by only one IRZ while the ORZ is lose reducing the equivalence ratio. The analysis will be mainly focused on the quantities able to describe the interplay between the aerodynamics of the flame and the flame: velocity vectors, temperature and OH with the latter acting as a marker of the hot gas presence.

Results and discussion

In this section, the post-processing of the two lean-blow out limit conditions will be presented separately. The discussion will start with the analysis of the H1 condition characterized by higher bulk velocity. There is a plenty of combinations among different quantities that could be presented to investigate the flame extinction; additionally,

several POD/E-POD modes could be deeply analyzed. For sake of brevity, the results that will be presented are limited only to the most significant modes among the first four: it has been verified that the others do not play a significant role in the description of the flow-flame interaction, being associated to coherent structures with low energy content.

This section is organized as follows: the first part defines the number of snapshots required to have an independency of the results in terms of energy content of the first two modes and peak frequency. The second part will be dedicated to the analysis of the test point H1 with the goal to identify the main coherent structures and their interaction with the stabilization zones. Lastly, it will be analyzed how the latter change reducing the bulk velocity along the P3 condition.

Sensitivity analysis for the definition of the number of modes

The first parameter to be fixed is the number of modes to be considered in the calculation of the truncated correlation matrix, having $N = 920$. The decision is made performing the POD of the axial velocity on the longitudinal plane and calculating both the energy content and the dominant frequency for the first two modes. According to Figure 5, it can be noticed that the energy content of these modes is not subjected to drastic changes considering a minimum amount of eigenvalues equal to 350, with the turbulent kinetic energy remaining close to 6% and 3.5% of the total for the first and the second mode, respectively.

Analogously, Figure 6 summarizes how much the peak frequency of the eigenvector spectra fluctuates with $\check{N}$. The first POD mode is characterized by a constant dominant frequency taking just more than 250 modes into account. The second mode is subjected to stronger variations with the analysis suggesting that a relevant number of modes cannot be smaller than 300. Based on this findings, 500 modes are considered for all the following analysis.

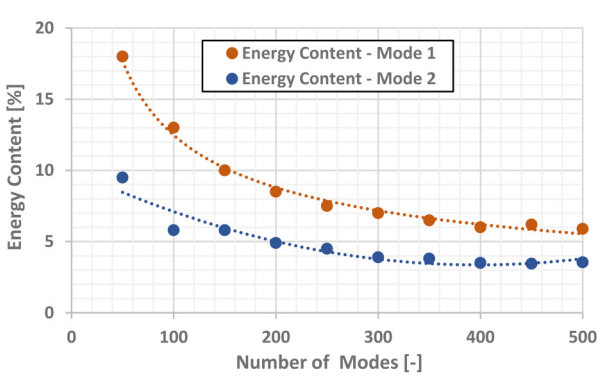

Figure 5. Turbulent kinetic energy content associated to the first two POD modes of the axial velocity calculated on the longitudinal plane of the computational domain varying the total number of modes.

Analysis of the H1 condition

A deep investigation is firstly dedicated to the correlation between the temperature and the velocity field at the burner exit (PL1 location) where the root of the flame is anchored. According to Figure 4, the $y - z$ velocity components are considered for the calculation of the orthonormal base onto which the temperature field is projected for the calculation of the E-POD. Figure 7 reports the most relevant information in terms of both spatial and temporal extended modes for the first 5 coherent structures. The analysis of the spatial modes reveals that the regions where the temperature is mostly synchronized with the velocity field are not evenly distributed along the exit anulus. This means that the temperature response to the fluctuation of the coherent structures has some preferential directions that are different for each mode. While this aspect will be further discussed later (Figure 8), it is here important to focus the discussion on the temporal modes.

From the E-POD theory, the temporal coefficients are the result of the standard POD analysis of the principal base, i.e., Vy, Vz in this case. From both the reported time history and the corresponding FFT, it is clear that each mode is characterized by the spread of the energy content all along the frequency spectrum. Additionally, the peak frequencies are in any case higher (M1, M3, M5) or close (M2, M4) to 2 kHz. Such findings suggest that the velocity field and consequently the associated fluctuations of the temperature are mainly characterized by the turbulent fluctuations at the flame root. This demonstrates that, despite the combustor is operating at the edge of the LBO curve, in such operating condition the combustion process is weakly affected by the aerodynamics at the anchoring zone and without any further equivalence ratio decreasing the flame maintains stable.

To better quantify these results, Figure 8 shows the maximum distortions the flame is subjected to. Each reconstructed E-POD mode is algebraically summed to the time averaged solution all along the collected time history and the two time frames where the flame shows the maximum deformation are here reported. For sake of brevity, only the modes M1, M2, and M4 are reported since it has been verified that modes 3 and 5 show deformations that are less significant than the ones here discussed. The vectors associated to the same POD modes of the velocity are reported as well: it can be seen that the regions where the identified coherent structures fluctuate coincide with the maximum deformation zones of the temperature E-POD. The red arrows reported in the picture identify the main directions along which these vortices stretch the flame. The intensity of these coherent structures changes during their own time evolution (according to the corresponding temporal base) and the reported contour plots of the temperature E-POD identify the positive and negative flame profile deformation. So, from this analysis, it can be

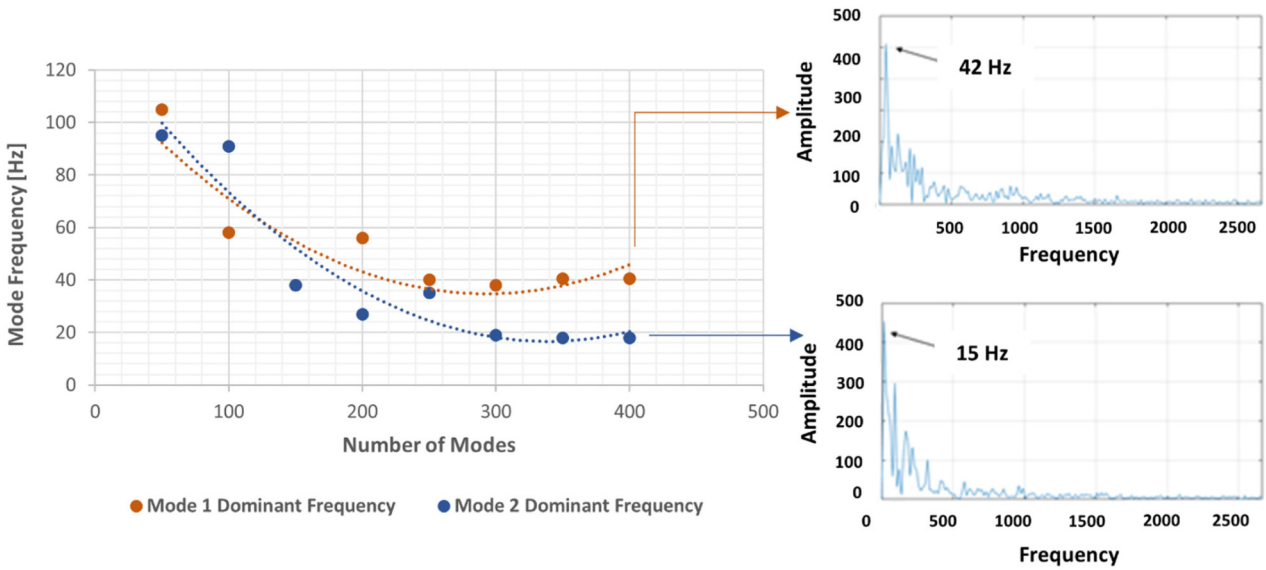

Figure 6. Mode peak frequency change with the number of modes.

observed that the E-POD modes M1 and M2 elongate the flame root such that a typical hexagonal shape of the temperature profile is assumed. This shape is due to coherent structures having an opposite position along the flame annulus and created by the axial swirler whose blades create six vanes. The main difference between these two modes is a different spatial phase since, as previously stated, the modes act on different regions of the flame front. On the contrary mode, M4 seems to have fewer preferential directions in the flame stretch, located mainly in the left-bottom side of the plane P1: as a matter of fact, the remaining portions of the flame front do not highlight significant profile changes during the time evolution.

In any case, this analysis suggests that, despite the flame profile is wrinkled by the identified vortices, there is still a strong anchoring region represented by the high temperature core sustaining the heat release inside the IRZ. As clearly visible from Figure 8 and differently from the operating conditions far from the LBO limits characterized by the presence of hot products also in the ORZ,[3,13,21–30] in this case the operability of the flame is ensured exclusively by the IRZ. So, in order to retrieve some clues of the destabilizing mechanism leading to the loss of flame, the discussion will be focused on the analysis of the IRZ and its interaction with the velocity field.

At this scope, the same kind of post processing is replicated on both the longitudinal mid-plane and the cross-section PL2, the latter able to investigate the solution inside the IRZ.

Figure 9 presents on the left-hand side the time average field of the temperature and the vectors of the first velocity POD mode (mean position of the $x-y$ velocity components); on the right-hand side, the effect of the first temperature E-POD mode onto the time average solution is reported instead. Looking at the velocity vectors, it can be noticed that the first mode is characterized by strong vortices located at the end of the cold mixture plumes but, more importantly, by some macro structures whose preferential directions bring the gases to recirculate toward the burner exit (identified by the red arrow in the picture). At the same time, the E-POD of the temperature highlights two main phenomena. Firstly, the first mode produces a periodic transversal stretch of the IRZ: the hot products are alternatively subjected to a strong compression and dilatation resulting in a maximum variation of the mean temperature of about 100 K in the center line. This strong fluctuation is responsible of an important weakening of the stabilizing region of the combustion. Secondly, when the maximum longitudinal contraction happens, in the regions where the flow is subjected to the reverse flow the temperature gets lower. This means that in addition to the periodic weakening of the IRZ, there is also the ingestion of colder products toward the premixer direction. The periodicity of such effects is summarized by the time history and the corresponding FFT of the time coefficients in the bottom side of the picture: being the E-POD built on the velocity base, these results are valid for both the velocity vectors and the temperature. From these graphs, it can be observed that the system fluctuations show a low-frequency peak close to 100 Hz. This value is typical of the highly premixed flame approaching the extinction, demonstrating that the proposed methodology is able to correctly capture the physics of the problem. Looking at the burner exit, it can be noticed that the flame morphology is not subjected to sudden variations with the opening angle of the flame front showing a negligible change over the time. This

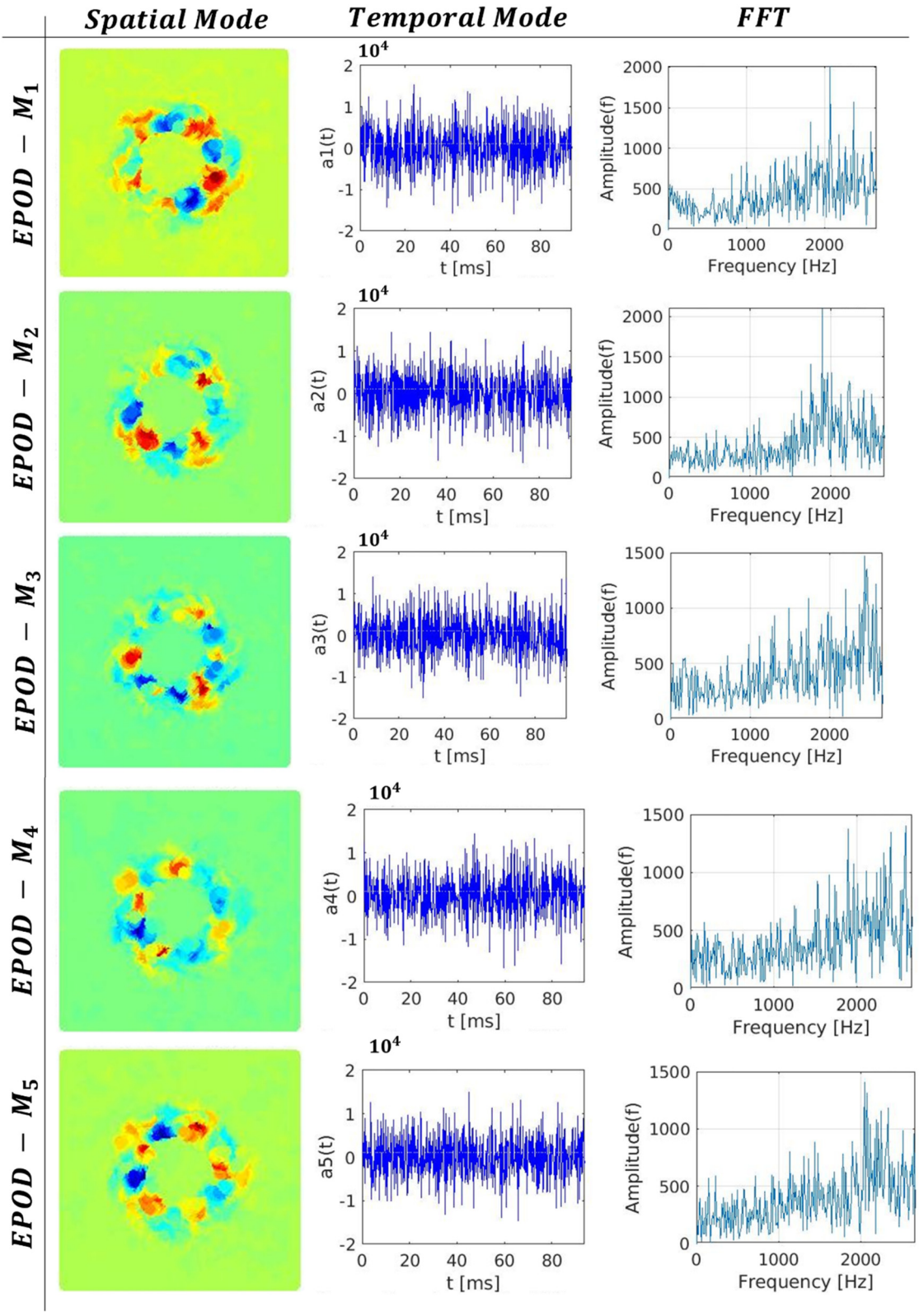

Figure 7. H1: Extended-POD of the Temperature along the Vy,Vz base for the first 5 modes. From left to right: spatial modes, temporal modes and the corresponding FFTs. Spatial modes are reported with an arbitrary scale where blue is the minimum value and red the maximum.

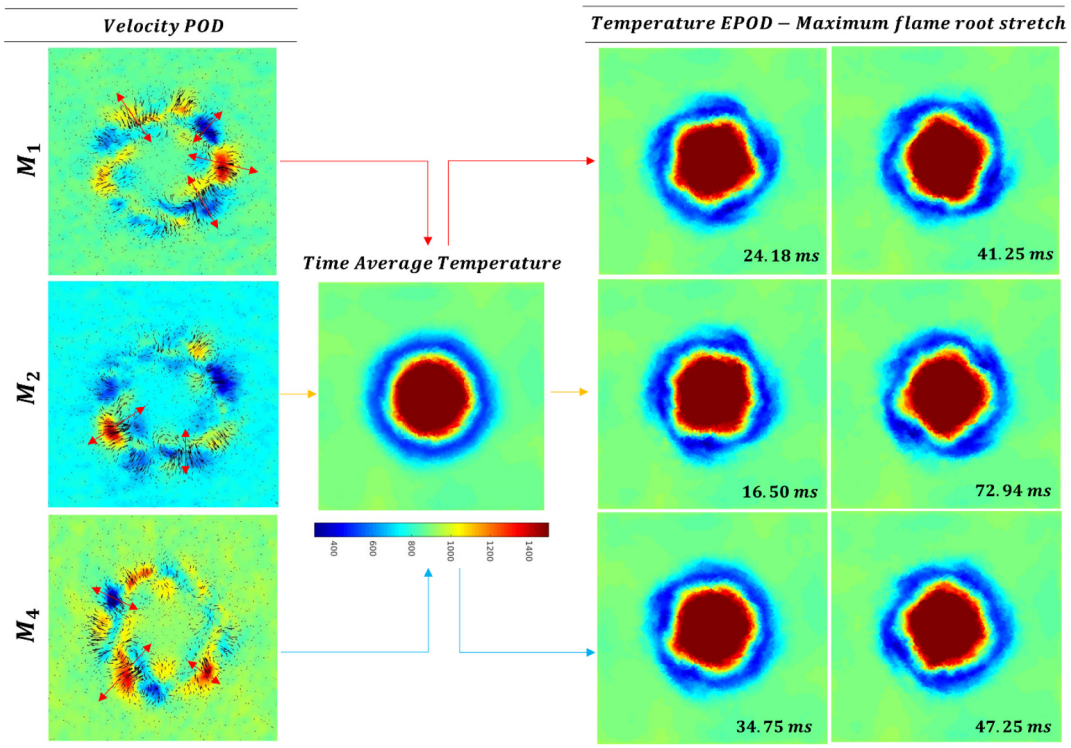

Figure 8. H1: Interaction between the velocity POD modes and maximum wrinkling of the time-average temperature profile for the modes M1, M2, and M4.

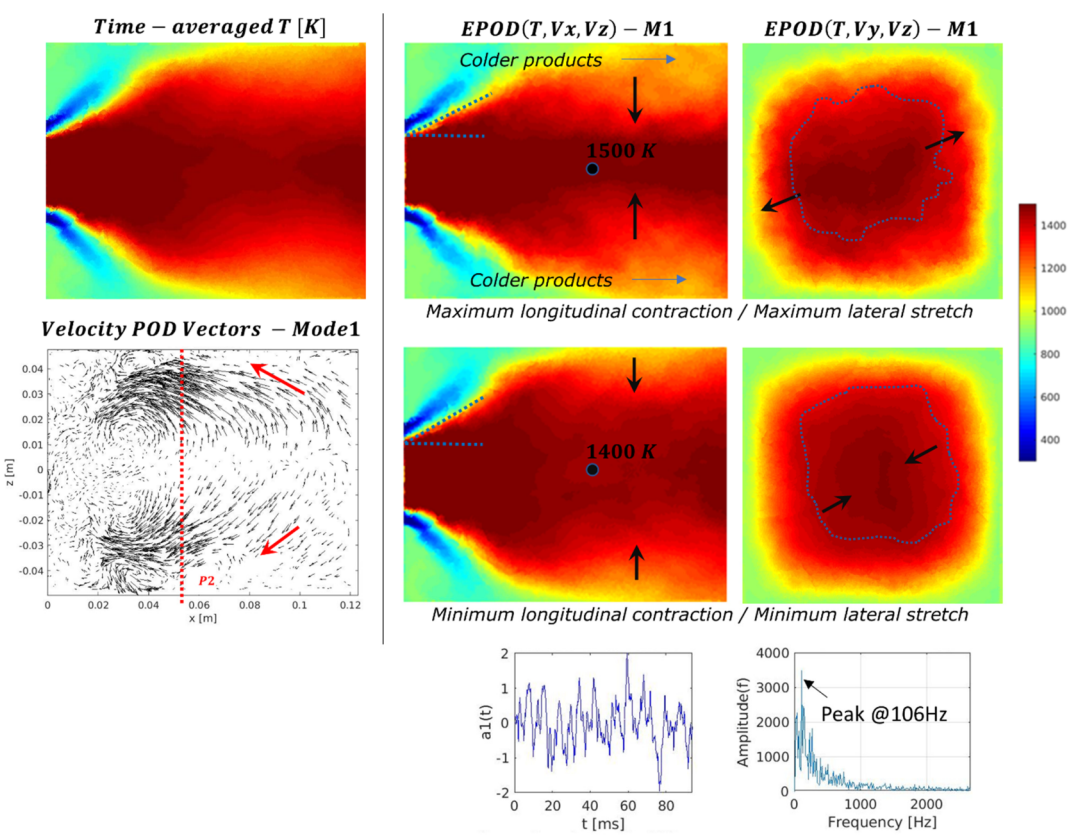

Figure 9. Joint effect of the velocity and temperature fluctuations on the IRZ. The EPOD plots represent the sum of the time averaged temperature and the first mode. The phenomena are characterized by a periodicity having a peak of 106 Hz. M1 has an energy content of about 6%.

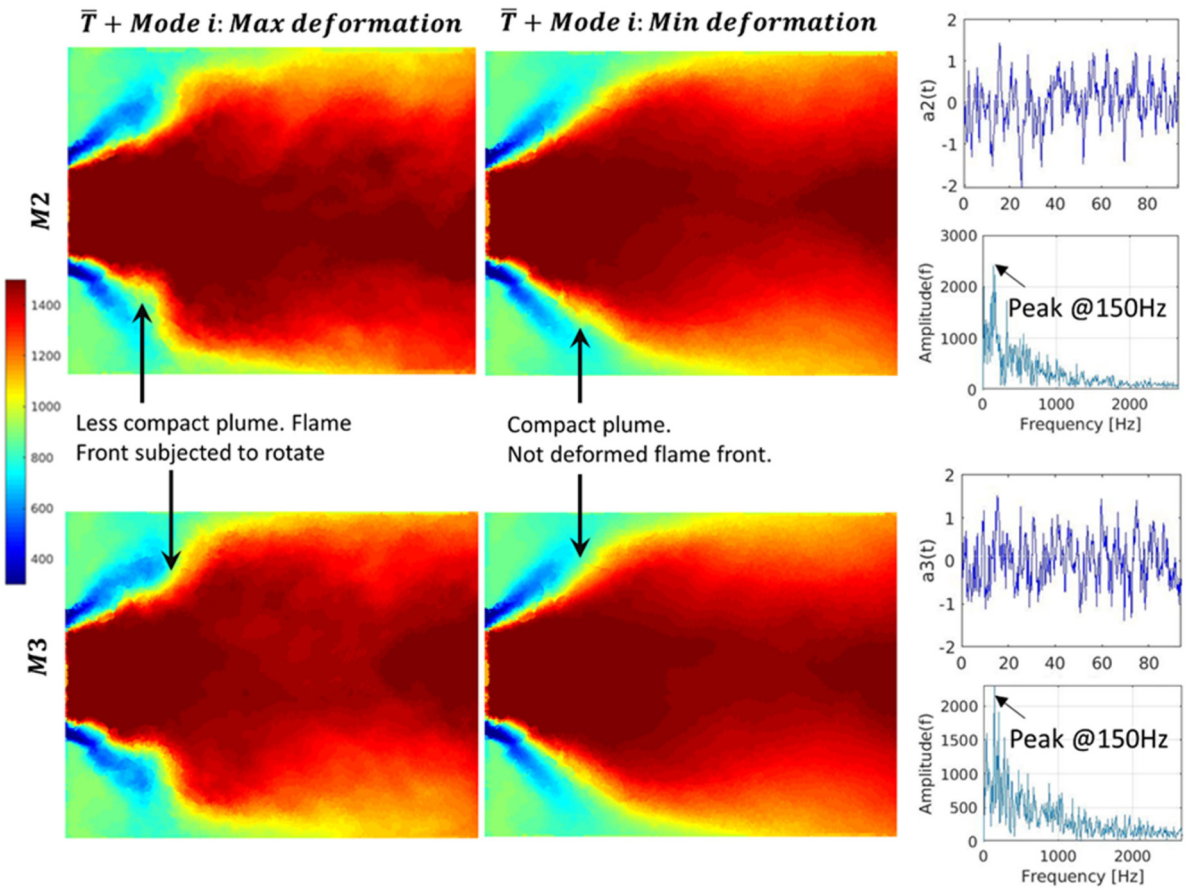

Figure 10. Mean temperature maximum and minimum deformation by M2 and M3 E-POD modes having an energy content of 4 and 3.5%, respectively. Time coefficients are multiplied by 10^4.

means that the first E-POD mode acts exclusively on the central part of the IRZ.

To complete the analysis, the right-hand side of the Figure 9 reports the first E-POD mode of the temperature (having 6% of the entire energy content) at PL2 location at the same instants. Such cross-section provides a clearer view of the hot products distribution inside the IRZ. It can be observed that, when the maximum longitudinal contraction occurs, the hot gases at peak temperature are stretched along a preferential diagonal direction that is completely missing when the longitudinal contraction reaches its own minimum. Moreover, a slight decrease of the temperature on the external regions (out of the iso-line at 1250 K) where the ingestion of colder products can play a role can be noticed.

Differently from the first mode, the second and the third ones (having 4% and 3.5% of the total fluctuating energy) directly act on the flame front close to the ORZ. Figure 10 identifies the maximum and the minimum deformation of the mean temperature field during the investigated time window. The two modes squeeze the flame morphology in the same way and in a symmetrical manner with respect to the combustor axis, resulting in a sudden lift of the front when the maximum deformation is reached. In this condition, the fresh mixture jets show a shorter penetration with a less compact shape. Both modes have the time coefficient spectra with a dominant frequency of 150 Hz and, additionally, they act in phase: for example, the pictures of Figure 9 consider the same time frame for M2 and M3 but such behavior has been verified to be general.

As reported in Figure 11, mode 4 shows the same kind of deformation characterizing both modes 2 and 3 even if the two sides of the flame are not stretched simultaneously. Instead, when one side is altered by the corresponding vortical structure, the other does not present any kind of distortion. Looking at the frequency spectrum, the peak is located at about 350 Hz, much higher than the other modes. Furthermore, the energy content of this mode is more uniformly distributed along the frequency spectrum in the range between 0 and 500 Hz compared with the graphs of the previous modes. This means that the fluctuating energy that begins to be modest (2.8%) compared to the energy of the M1 is spread over a significantly larger

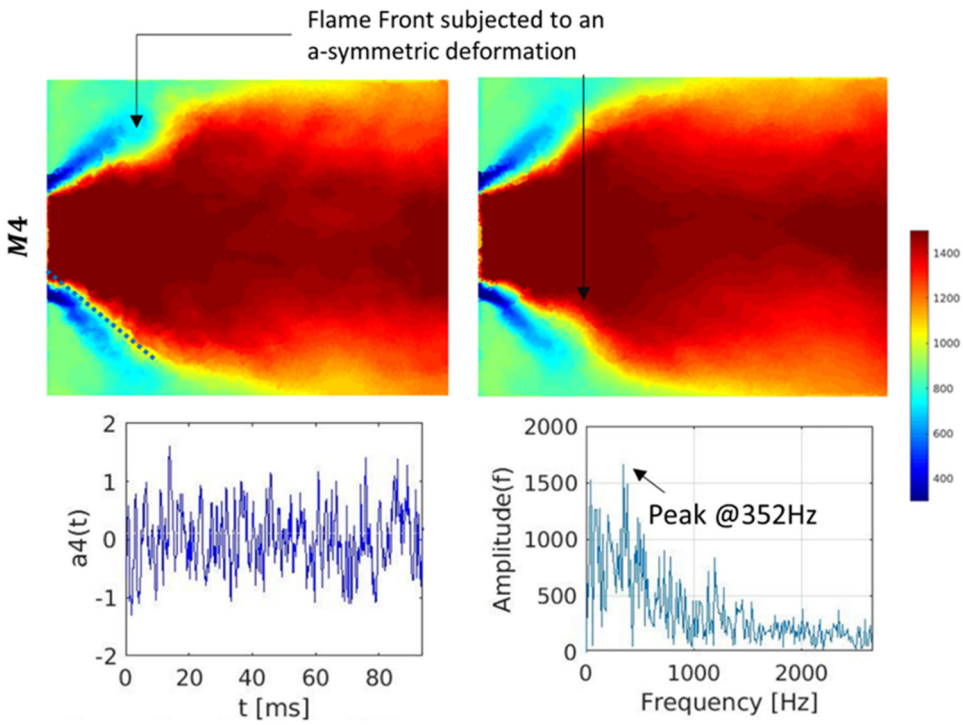

Figure 11. A-symmetric deformation of the temperature field operated by mode 4 whose energy content is equal to 2.8%. Time coefficient to be multiplied by 10^4.

range of frequency. Lastly, looking at the magnitude of the peak located at 350 Hz, it can be noticed that it is quite smaller compared to the amplitude of the previous three modes, demonstrating that higher order modes have an energy content that doesn't alter so much the behavior of the system

For completeness, Figure 12 plots the E-POD analysis of the OH field on plane PL2. The results obtained for such species are formally identical in terms of flame morphology and deformation to the ones obtained for the temperature. As a consequence, the first mode has been omitted, since it has been already included in Figure 9. The main advantage of OH with respect the temperature is that it makes the flame distortions more detectable and visible.

For each mode, Figure 12 reports the spatial distribution and the time coefficients. About the former, the main directions through which the coherent structures act are highlighted. Mode 4 and more importantly mode 2 have diagonal preferential directions around which the IRZ is compressed and stretched. This finding is more evident from the sum of the time average OH solution and the reconstructed mode, reported on the right-hand side of the figure. Also, from this analysis, it can be noticed that the mode 4 is the only one having a hybrid behavior: one deforming direction is of diagonal type, the other is lateral. On the contrary, mode 3 seems to deform the IRZ only on the lateral sides. All these modes manifest also in this case quite low dominant frequencies, ranging from 106 Hz (M2) to 138 Hz (M3 and M4). Regarding M4, analogously with what has been observed for the temperature field, also in this case it can be noticed that:

(a) the peak of the time coefficient spectrum is lower than in the lower-order modes;
(b) higher excited frequency compared to lower order mode (138 Hz vs 106 Hz);
(c) in the range 0–500 Hz, the distribution of the time coefficient spectrum has low-frequency contributions.

Considering the OH concentration as marker of hot gas products, it can be understood how both the core of the IRZ and the lateral portions of the section are interested by large low-frequency fluctuations of the temperature if compared with the mean solution. Furthermore, it is interesting to notice that when the maximum stretch of the flame shape is reached, the OH mass fraction associated to any single mode is lower than the mean value in the external parts, closer to the quartz. This is another proof that, in these conditions, fresh gases coming from the outlet of the domain are ingested toward the burner.

Analysis of the P3 condition

As highlighted by Nassini et al.,[21] the bulk velocity reduction leads to a longer transition from a stable operating condition to the loss of flame. Considering the LBO curve

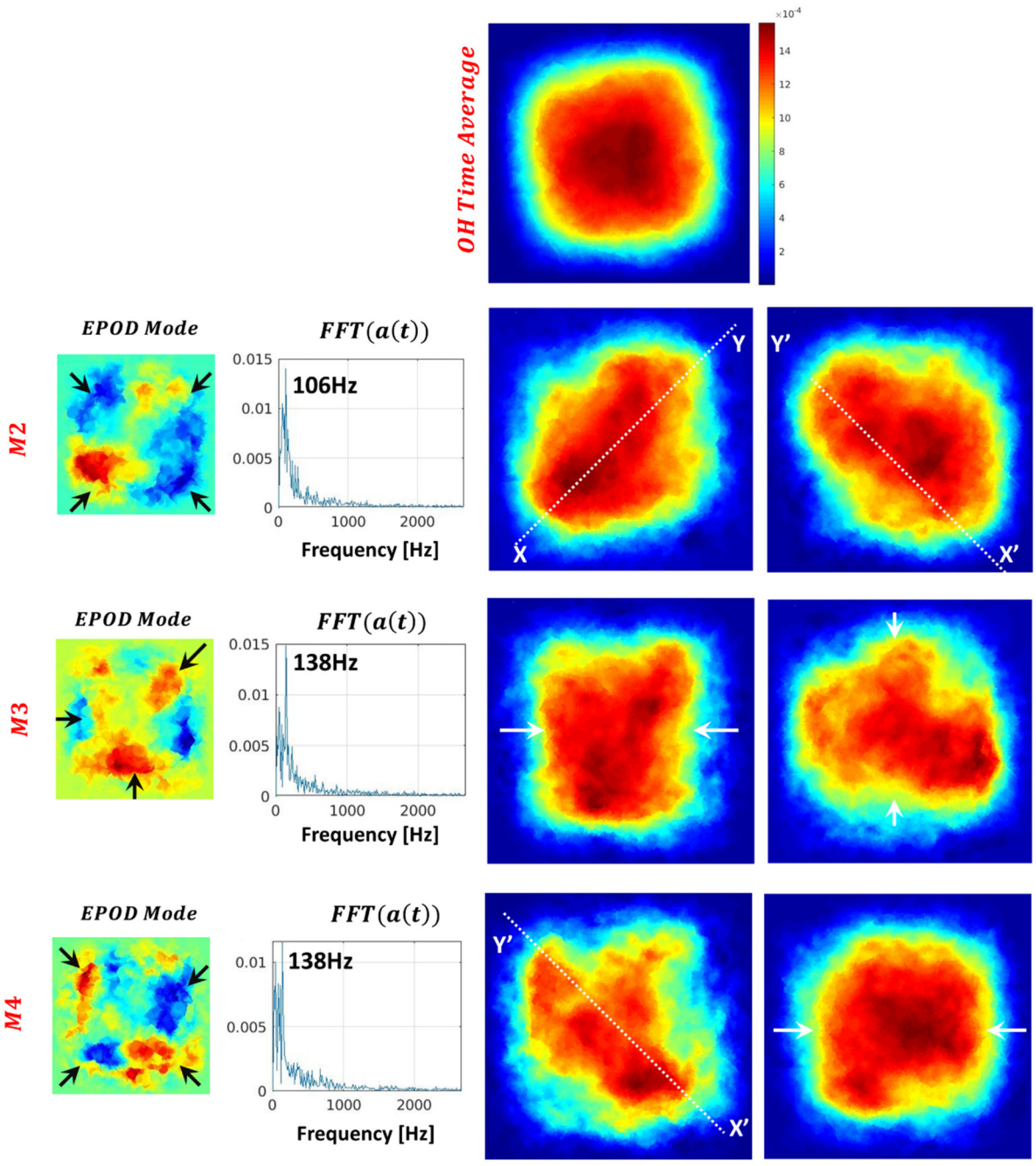

Figure 12. E-POD analysis of the OH mass fraction correlated to the velocity field for the modes from 2 to 4. The two frames at the maximum level of distortion of the time averaged solution are reported. All the modes act in a low frequency range above 100 Hz.

reported in Figure 3, when the flame is subjected to the same equivalence ratio reduction, it takes approximately 275 ms to extinguish in "P-like" condition while only 150 ms are sufficient in "H-like" condition. Figure 13 summarizes such findings reporting the volume-average temperature inside the combustor. This outcome could be related to the lower aerodynamic strain acting on the fully premixed flame in P-like condition, considering also the lower equivalence ratio.

Nevertheless, the same analysis performed for H1 test point is repeated also for P3 to identify the differences in terms of flow-flame interaction and their role in changing the flame morphology approaching the loss of flame. For sake of brevity, only the most evident findings will be here reported and discussed.

The first significant difference between the two operating conditions is visible looking at the time-averaged temperature fields (Figure 14). P3 is characterized by

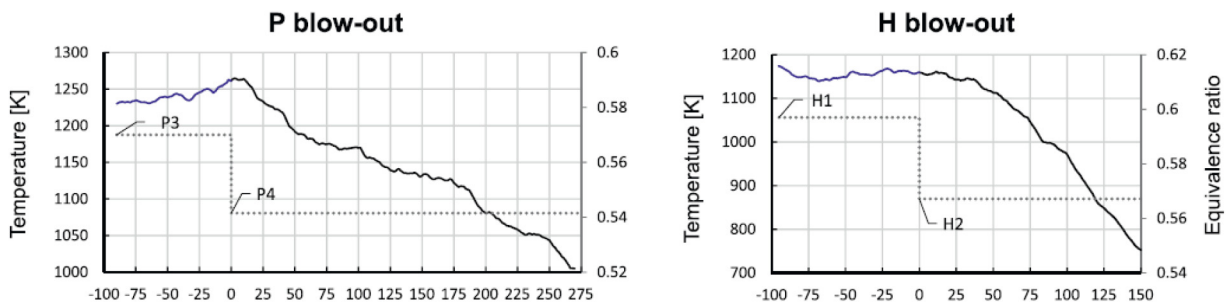

Figure 13. Time histories of the combustor volume-average temperature from the last stable operating condition till the flame extinction for the two test points after the equivalence ratio reduction.[21]

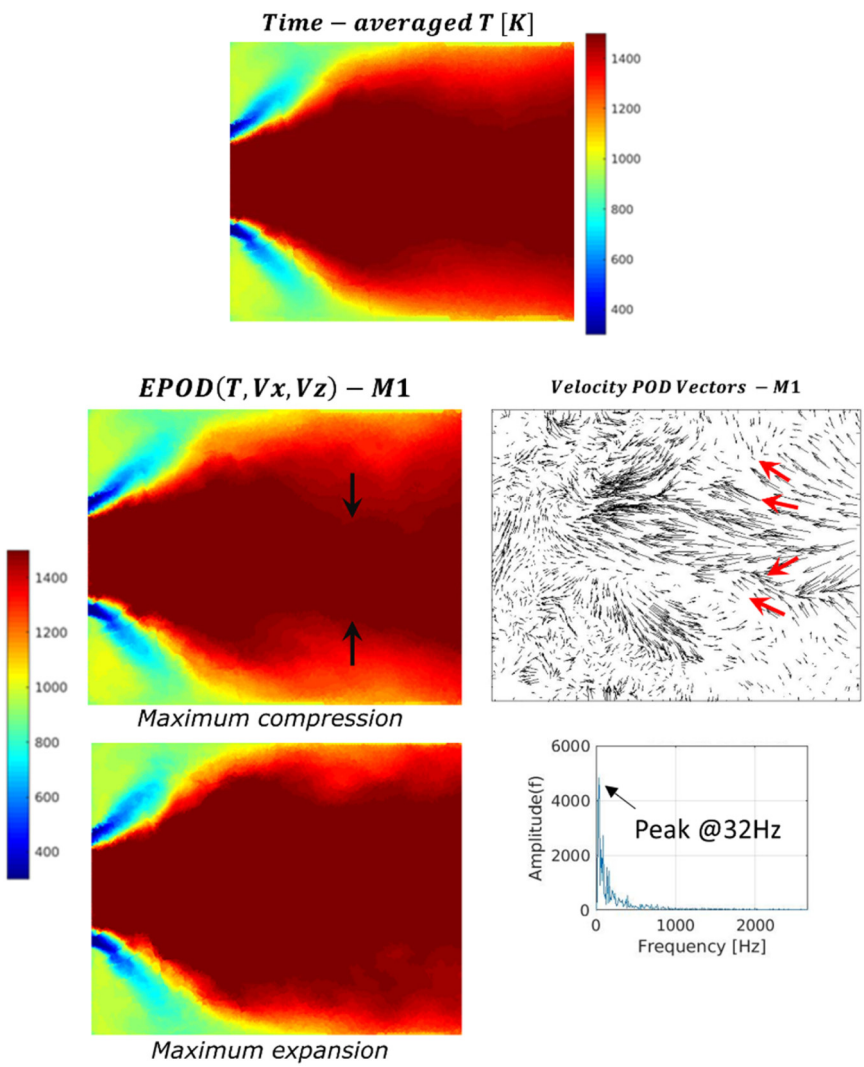

Figure 14. P3 test point. Mean temperature field (top) and its maximum deformations related to the first E-POD mode where the extended POD is performed considering the velocity field on the longitudinal plane (bottom).

the presence of hot combustion products ($T > 1400\ K$) all along the IRZ while, as visible from Figure 9, the mean temperature is affected by a sudden temperature drop in the core region of the combustor for H1. This can be seen as a clue of a more robust stability operating with lower bulk velocity (P3 flame). Furthermore, the stronger recirculation region in P3 is less affected by the interaction with the velocity field than in H1. Considering

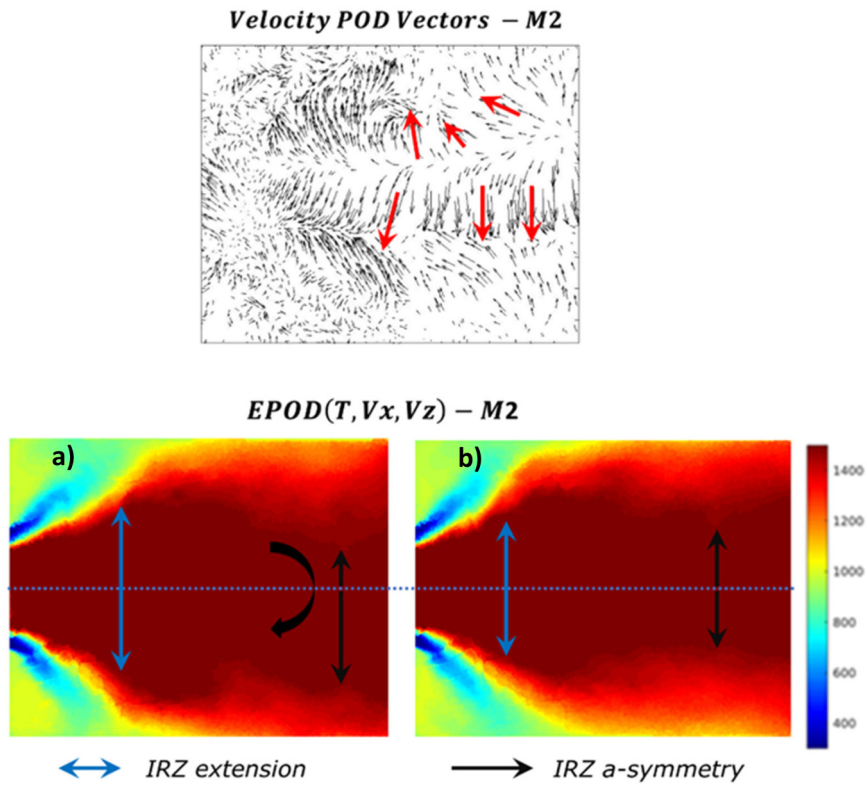

Figure 15. Mean temperature field deformation due to the second E-POD mode. The blue arrows detect the radial contraction/expansion of the recirculation zone leading to a change of the solid angle of the flame; the rotational effect is highlighted by the black arrow.

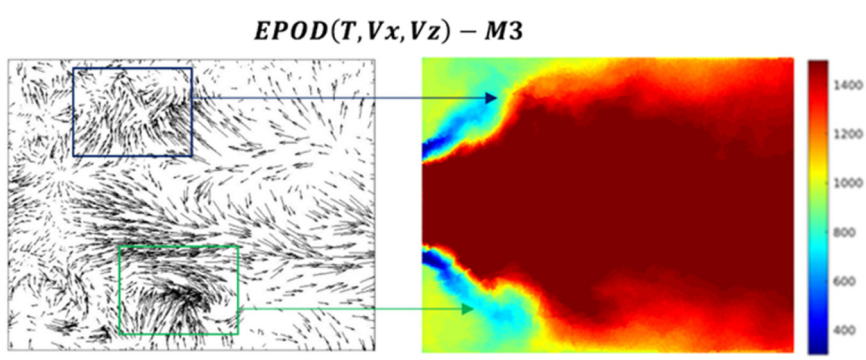

Figure 16. Mean temperature solution + E-POD mode 3: the two external vortical structures wrinkle the flame front.

the first E-POD mode on the combustor mid-plane, its fluctuations are not able to break the IRZ hot core. The velocity vectors of the first mode identify a preferential direction close to the end of the investigated window (red arrows in the picture) responsible of a low-frequency (32 Hz) radial stretch of the IRZ. Despite this effect, even when the flame is subjected to the maximum compression, the IRZ never suffers breaks or discontinuities and also the external regions responsible for the ingestion of colder products identified for H1, are limited.

The first as well the second E-POD mode do not show any effect on the flame brush downstream the swirler exit. Instead, the second E-POD mode acts again on the IRZ in two different ways. Firstly, a radial contraction-expansion can be identified. As a result, the solid angle of the IRZ is subjected to a slightly change along the 85 Hz frequency characterizing this mode (blue arrow in Figure 15). Secondly, the position of the hot products far downstream the IRZ is subjected to an asymmetric rotation: with respect to the center line of the combustor, the flame

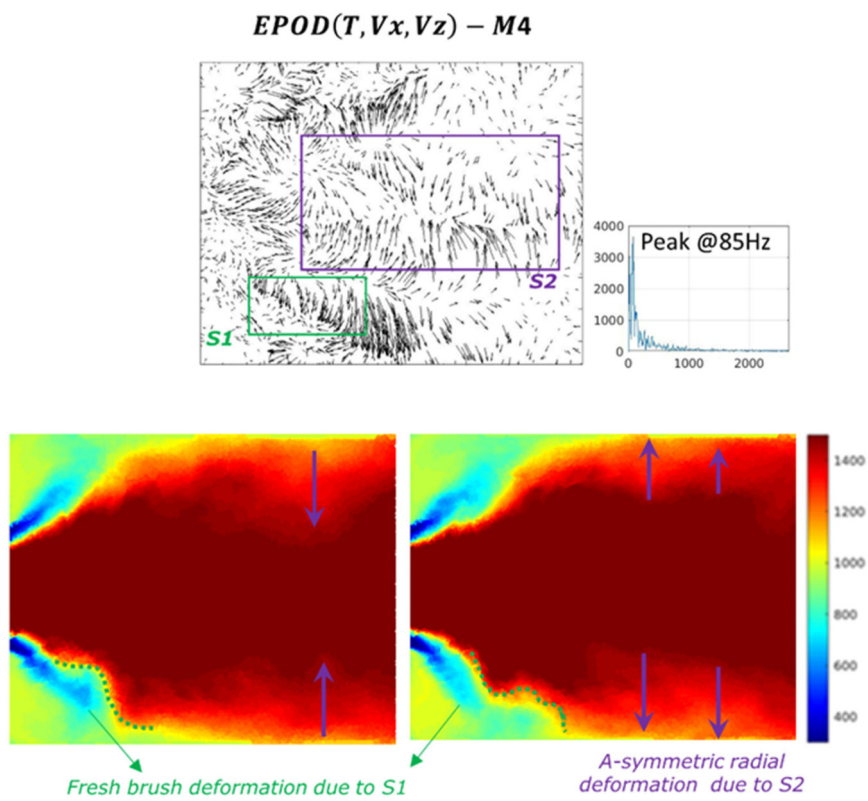

Figure 17. Mean temperature solution + E-POD mode 4 responsible for both a local impact on the flame front and a radial deformation of the core.

oscillates alternatively from the position reported in Figure 15 to a configuration that is quite similar to the mean solution (Figure 15).

The presence of two different vortical structures identified by the third E-POD mode and located in the outer portions of the combustor are responsible for the deformation of the flame brush. Especially in the bottom part of the chamber, the vortex is able to significantly wrinkle the flame: Figure 16 reports the time frame when the maximum deformation of the time averaged solution is reached. At this instant, even the cold plume of the reactants is impacted by this effect, with an elongation in the axial direction if compared to the plume structure on the opposite part of the combustion chamber. In any case, this can be considered as a local interaction that does not play a crucial role in the global behavior during this operating condition.

The 4th E-POD mode reveals two main structures deforming the flame. The first one, S1, has a similar effect on the flame brush than the one just described for M3. More importantly, the IRZ is stretched in the same way and at the same frequency (85 Hz) analyzed for the 2nd E-POD mode. Also in this case, the coherent structure S2 induces an a-symmetry of the recirculation zone with respect to the center line of the system, as depicted in Figure 17.

Figure 18 reports the analysis in terms of OH mass fraction on the cross-plane PL2; analogously to what has been presented in Figure 12, the main E-POD modes and the maximum deformations they produce onto the time average field are presented. First of all, the comparison of the mean solutions highlights critical differences between the two operating conditions. While H1 is characterized by a peak of Y_{OH} only in the central part of the section, a wider radial extension of the region at high OH concentration is present for P3. Additionally, H1 is affected by a rougher decay of Y_{OH} from the center of the section to the external part of the combustor.

These differences can be explained looking at the structures of the OH mass fraction synchronized with the velocity field. As reported in Figure 18, the first E-POD modes of OH (M1, M3, and M4) do not highlight any preferential direction significantly stretching the time average distribution. Differently from what discussed in Figure 12, for P3 condition the morphology of the OH mass fraction is neither stretched nor twisted such that the global spatial and temporal distribution of the combustion products leads to a weakening of the stabilization region. The iso-lines at Y_{OH} = 1.4e-04 are drawn in the regions where the coherent structures of the flow (reported in the first column of the figure) produce their maximum effect of distortion helping to highlight that even in these instants the stability of the combustion is not compromised.

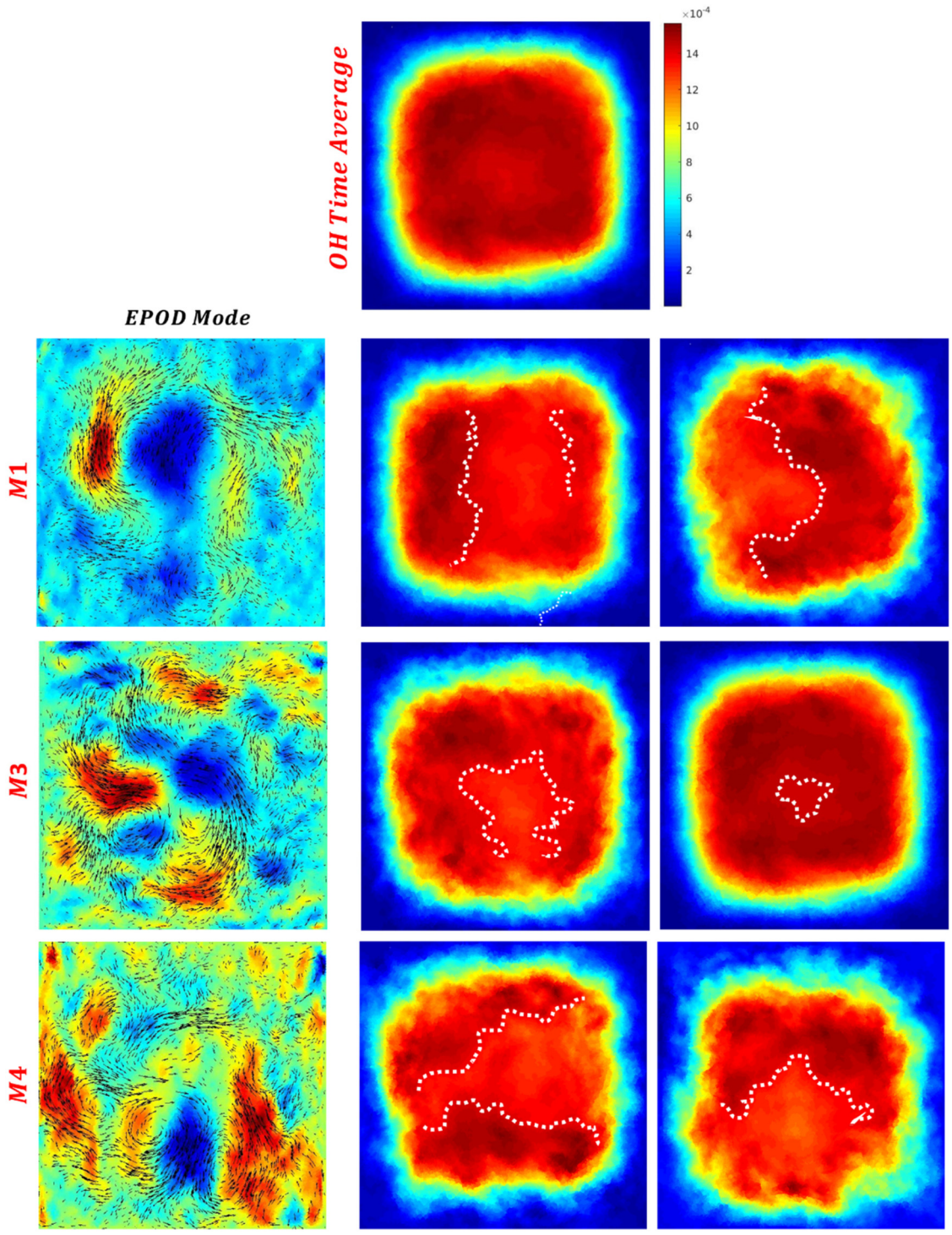

Figure 18. E-POD of the OH on plane P2. Effect of the modes M1, M3, and M4 onto to the time average solution. Mode M2 not reported due to its weak impact. White iso-lines at 1.4e-04.

Conclusions

The complex physical mechanisms leading to the lean blow out of a perfectly premixed combustion system operating at atmospheric pressure has been investigated through a LES based model where the inclusion of the strain rate and heat loss effects are embedded into the combustion model. Leveraging the validation against the experimental data at two different operating conditions, the numerical model has been used to collect the several quantities at

different planes trying to shed some light on the flow-flame interaction.

After a preliminary analysis for determining the minimum number of modes to be considered, the application of the E-POD algorithm to the quantities relevant for the stability of the system (temperature and OH mass fraction) has been used to highlight the differences between the two operating conditions. It has been found that, when the rig is operated with a higher bulk velocity, despite the higher equivalence ratio:

- the IRZ, responsible for the flame stability, is subjected to a cyclic low-frequency break down;
- the ingestion of cold products is enhanced by the presence of coherent structures acting mainly in the external parts of the combustor.

On the other hand, the flame with lower bulk velocity features weaker alterations of the IRZ, and even when the flame is subjected to the maximum deformation the central region of hot products never suffers breaks or discontinuities. This aspect is crucial as the ingestion of colder products, occurring from the IRZ sides in the higher velocity flame, are considerably limited, enhancing the flame stability. This observation appears to be the main reason causing the slower extinction transient observed by Nassini et al.[21]

More local effects acting on the flame brush have been found in both the operating conditions thanks to the modes calculated by means of E-POD. They are related mainly to higher order coherent structures of the flow field with a lower energy content, and their impact onto the flame stability is found to be of secondary importance since their interaction with the flame anchoring is quite limited. Nevertheless, their identification remarks that the E-POD can potentially capture hidden or secondary effects which are not easy to be observed by a direct interpretation of the simulation results.

Declaration of conflicting interests

The author(s) declared no potential conflicts of interest with respect to the research, authorship, and/or publication of this article.

Funding

The author(s) received no financial support for the research, authorship, and/or publication of this article.

ORCID iD

Antonio Andreini https://orcid.org/0000-0002-7508-9607

References

1. Schmid P. Dynamic mode decomposition of numerical and experimental data. *J Fluid Mech* 2010; 656: 5–28.
2. Rowley C, Mezić I, Bagheri S, et al. Spectral analysis of nonlinear flows. *J Fluid Mech* 2009; 641: 115–127.
3. Taira K, Brunton SL, Dawson STM, et al. Modal Analysis of Fluid Flow: An Overview. *AIAAJ* 2017; 55: 4013–4041. doi:10.2514/1.J056060
4. Sieber M, Oliver Paschereit C and Oberleithner K. Advanced Identification of Coherent Structures in Swirl-Stabilized Combustors". *ASME.J. Eng. Gas Turbines Power* 2017; 139. https://doi.org/10.1115/1.4034261
5. Gomez-Ramirez D, Ekkad SV, Moon HK, et al. Isothermal coherent structures and turbulent flow produced by a gas turbine combustor lean pre-mixed swirl fuel nozzle. *Exp Therm Fluid Sci* 2017; 81: 187–201.
6. Carlsson H, Carlsson C, Fuchs L, et al. Large eddy simulation and extended dynamic mode decomposition of flow-flame interaction in a lean premixed low swirl stabilized flame. *Flow Turbulence Combustion* 2014; 93: 505–519.
7. Huang C, Anderson WE, Harvazinski ME, et al. Analysis of self-excited combustion instabilities using decomposition techniques. *AIAA J* 2016; 54: 2791–2807. https://doi.org/10.2514/1.J054557
8. Meloni R, Ceccherini G, Michelassi V, et al. Analysis of the self-excited dynamics of a heavy-duty annular combustion chamber by large-eddy simulation. *J Eng Gas Turbines Power* 2019; 141. doi:10.1115/1.4044929
9. Noack B, Stankiewicz W, Morzyński M, et al. Recursive dynamic mode decomposition of transient and post-transient wake flows. *J Fluid Mech* 2016; 809: 843–872. doi:10.1017/jfm.2016.678
10. Duke D, Soria J and Honnery D. An error analysis of the dynamic mode decomposition. *Exp Fluids* 2012; 52: 529–542.
11. Syred N. A review of oscillation mechanisms and the role of the precessing vortex core in swirl combustion systems. *Prog Energy Combust Sci* 2006; 32: 93–161.
12. Huang C, Gejji R, Anderson W, et al. "*Combustion Dynamics Behavior in a Single-Element Lean Direct Injection (LDI) Gas Turbine Combustor*". 50th AIAA/ASME/SAE/ASEE Joint Propulsion Conference, AIAA, Paper 2014-3433, 2014.
13. Berkooz G, Holmes PJ and Lumley JL. The proper orthogonal decomposition in the analysis of turbulent flows. *Annu Rev Fluid Mech* 1993; 25: 539–575.
14. Duwig C and Fuchs L. Large eddy simulation of vortex breakdown/flame interaction. *Phys Fluids* 2007; 19. doi:10.1063/1.2749812
15. Petersson P, Wellander R, Olofsson J, et al. "*Simultaneous high-speed PIV and OH PLIF measurements and modal analysis for investigating flame-flow interaction in a low swirl flame*". 16th Int. Symp on Appl. Laser Techniques to Fluid Mechanics, Lisbon, Portugal, 2012.
16. Gadiraju S, Park S, Gomez-Ramirez D, et al. "*Application of Proper Orthogonal Decomposition to High Speed Imaging for the Study of Combustion Oscillations*". Proceedings of the ASME Turbo Expo 2017. Charlotte, North Carolina, USA. 2017. https://doi.org/10.1115/GT2017-64602.
17. Boxx I, et al. Temporally resolved planar measurements of transient phenomena in a partially pre-mixed swirl flame in a gas turbine model combustor. *Combust Flame* 2010; 157: 1510–1525.
18. Iudiciani P, Gutmark EJ, Hosseini SM, , et al. "Characterization of a Multi-Swirler Fuel Injector Using Simultaneous Laser

Based Planar Measurements of Reaction Zone, Flow Field and Fuel Distribution". Proceedings of ASME Turbo Expo 2009: GT2009-60278, Fairfield, NJ, 2009.
19. Borée J. Extended proper orthogonal decomposition: a tool to analyse correlated events in turbulent flows. *Exp Fluids* 2003; 35: 188–192.
20. Maurel S, Borée J and Lumley JL. Extended proper orthogonal decomposition: application to jet/vortex interaction. *Flow Turb. Combust* 2001; 67: 125–136.
21. Nassini PC, Pampaloni D, Meloni R, et al. *Lean blow-out prediction in an industrial gas turbine combustor through a LES-based CFD analysis*. *Combust Flame* 2021; 229, https://doi.org/10.1016/j.combustflame.2021.02.037
22. Shanbhogue SJ, Husain S and Lieuwen T. Lean blowoff of bluff body stabilized flames: scaling and dynamics. *Prog. Energy Combust Sci* 2009; 35: 98–120.
23. Muruganandam TM and Seitzman JM. Fluid mechanics of lean blowout precursors in gas turbine combustors. *Int. J. Spray Combust Dyn* 2012; 4: 29–60.
24. Kariuki J, Dawson JR and Mastorakos E. Measurements in turbulent premixed bluff body flames close to blow-off. *Combust Flame* 2012; 159: 2589–2607.
25. Meloni R, Chiarizia N, Andreini A, et al. "*Numerical Characterization of the Self-Excited Dynamics Behavior of a Technically Premixed Burner"*, Proceedings of ASME Turbo Expo 2022, GT2022-82248, Rotterdam, The Netherland, 2022.
26. Sirovich L and Kirby M. Low dimensional procedure for the characterization of human faces. *J. Opt. Soc Amer. A* 1987; 33: 591–596.
27. Duwig C and Iudiciani P. Extended proper orthogonal decomposition for analysis of unsteady flames. *Flow Turbulence Combust* 2010; 84: 25–47. https://doi.org/10.1007/s10494-009-9210-6.
28. Rajasegar R, Choi J, Ghanekar S, Mitsingas CM, Mayhew E, Liu Q, Yoo J and Lee T. "*Extended Proper Orthogonal Decomposition (EPOD) and Dynamic Mode Decomposition (DMD) for Analysis of Mesoscale Burner Array Flame Dynamics*". AIAA 2018-0147. https://doi.org/10.2514/6.2018-0147.
29. Cavaliere DE, Kariuki J and Mastorakos E. A comparison of the blow-off behaviour of swirl-stabilized premixed, non-premixed and spray flames. *Flow Turbul. Combust* 2013; 91: 347–372.
30. Nassini PC, Pampaloni D, Andreini A, et al. *"Large Eddy Simulation of Lean Blow-Off in a Premixed Swirl Stabilized Flame"*, Proceedings of ASME Turbo Expo 2019, GT2009-90856, Phoenix, USA, 2019.